

On numerical simulations of subaqueous slides: Back-calculations of laboratory experiments of clay-rich slides

Peter Gauer, Anders Elverhøi, Dieter Issler, & Fabio V. De Blasio

Gauer, P., Elverhøi, A., Issler, D. & De Blasio, F. V.: On numerical simulations of subaqueous slides: Back-calculations of laboratory experiments. *Norwegian Journal of Geology*, Vol. 86, pp. 295-300, Trondheim 2006. ISSN 029-196X.

To improve the understanding on the frontal behavior of submarine slides numerical simulations were performed to back-calculate laboratory experiments carried out at the St. Anthony Falls Laboratory, University of Minnesota. The slide and the ambient water are modeled by a two-phase model approach, which allows the study of the interaction between the slide and the ambient water. The presented simulations focus on clay-rich materials. They show the development of a high-pressure wedge of ambient water underneath the slide and of underpressure along its upper surface, which, in agreement with the laboratory experiments, leads to a hydroplaning head. In addition, a velocity decrease from the head to the tail of the slide could be observed, which leads to stretching of the slide mass. Stretching and thinning of the slide contributes to the softening of the material and may lead to progressive detachment of the head and development of out-runner blocks.

Peter Gauer, Norwegian Geotechnical Institute/International Centre for Geohazards, Sognsveien 72, NO-0806 Oslo, Norway (e-mail: pg@ngi.no); Anders Elverhøi, Dept. of Geosciences, University of Oslo, PB 1047 Blindern, NO-0316 Oslo, Norway & International Centre for Geohazards, c/o NGI, Sognsveien 72, NO-0806 Oslo, Norway (e-mail: anders.elverhoi@geologi.uio.no); Dieter Issler, Norwegian Geotechnical Institute/International Centre for Geohazards, Sognsveien 72, NO-0806 Oslo, Norway (e-mail: di@ngi.no) & Fabio V. De Blasio, Dept. of Geosciences, University of Oslo, PB 1047 Blindern, NO-0316 Oslo, Norway & International Centre for Geohazards, c/o NGI, Sognsveien 72, NO-0806 Oslo, Norway (e-mail: fvb@ngi.no)

Introduction

Submarine slides can reach enormous runout distances on slopes with only a few degrees inclination, as can be seen by the ancient Storegga slide showing a runout of about 800 km on a slope with a mean angle of less than 1° (Bryn et al. 2005) or in the case of the more recent Grand Banks event from 1926, which extended more than 1000 km (Locat & Lee 2002). These observed long runout distances are not explainable with simple rheological models based on measured in situ (remolded) soil properties. However, in-depth understanding of this phenomenon is one of the urgent needs for risk assessment for coastal regions and offshore constructions. An overview of the current understanding of submarine slides is found in the above-mentioned article by Locat & Lee (2002) and also in (Elverhøi et al. 2005). Both articles emphasize the frontal behavior as one key factor for the understanding of long runouts. This paper focuses on numerical simulations of clay-rich subaqueous slides and their comparison to laboratory experiments. It is a step towards a more detailed study of the frontal behavior of slides.

Numerical model

In this section, we give a brief description of the numerical model approach used for the back-calculation of

the laboratory experiments. The slide and the ambient water are modeled by a two-phase model (see Figure 1). For both, the slide and the ambient water, the continuity equation and momentum equation are solved. The water is considered as a turbulent flow that needs a turbulent closure. In the presented case, the rheological behavior of the slide is described as a Bingham fluid with a constant yield strength and consistency (Bingham viscosity). The model is implemented in the commercial flow solver CFX4 from ANSYS (CFX4.3, 1999),

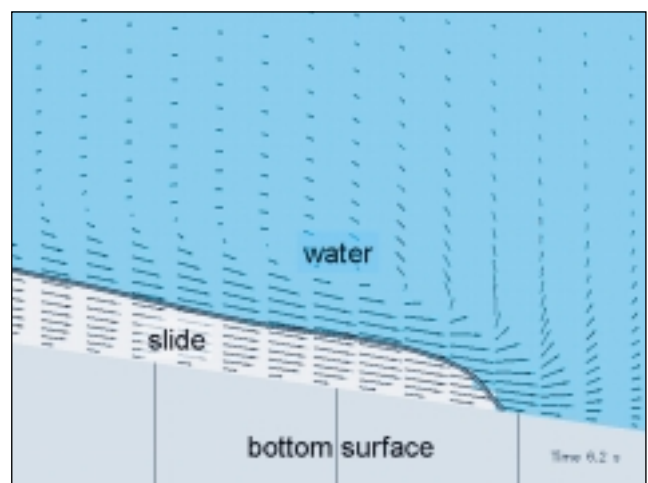


Fig 1: Schematic representation of the model approach. The bold black line marks the interface between the water and the slide phase (isosurface of volume fraction; $v_w = v_s = 0.5$). Vectors indicate the barycentric velocity field.

which uses a finite volume approach. The sliding mass is assumed to be sufficiently wide so that a two-dimensional (vertical) treatment can be justified.

Governing equations

The mass balance for ambient water (marked with the subscript w) and the one for the slide (marked with the subscript s) can be written in the form

$$\frac{\partial v_w \rho_w}{\partial t} + \nabla \cdot (v_w \rho_w \mathbf{V}_w) = 0, \quad (1)$$

$$\frac{\partial v_s \rho_s}{\partial t} + \nabla \cdot (v_s \rho_s \mathbf{V}_s) = 0, \quad (2)$$

where \mathbf{V} is the velocity, ρ the intrinsic density of the respective phase, and v_w and v_s are the volume fractions of the water and slide, respectively ($v_w = 1 - v_s$). $\partial/\partial t$ denotes the local differentiation in time and ∇ is the gradient operator. The momentum equation for the ambient water reads

$$\frac{\partial v_w \rho_w \mathbf{V}_w}{\partial t} + \nabla \cdot (v_w \rho_w \mathbf{V}_w \otimes \mathbf{V}_w) = -v_w \nabla p + \nabla \cdot [v_w \mu_w (\nabla \mathbf{V}_w + (\nabla \mathbf{V}_w)^T)] + v_w \rho_w \mathbf{g} - \mathbf{D}_{ws}, \quad (3)$$

here \otimes indicates the tensor product, p is the common pressure, \mathbf{g} the gravitational acceleration. The effective viscosity of water, μ_w , is given by

$$\mu_w = \mu_l + \mu_t, \quad (4)$$

where μ_l is the laminar viscosity and μ_t the turbulent viscosity. In this case, either the standard k- ϵ (Rodi, 1989) or a LES (Ferziger & Peric 1999) approach is used for the turbulent closure. The last term on the right hand side in Equations (3) and (5) describes the mutual drag between the slide and the ambient water (opposite in contribution in the respective phase). The momentum equation for the slide reads as follows

$$\frac{\partial v_s \rho_s \mathbf{V}_s}{\partial t} + \nabla \cdot (v_s \rho_s \mathbf{V}_s \otimes \mathbf{V}_s) = -v_s \nabla p + \nabla \cdot [v_s \mu_s (\nabla \mathbf{V}_s + (\nabla \mathbf{V}_s)^T)] + v_s \rho_s \mathbf{g} + \mathbf{D}_{ws}, \quad (5)$$

For the coupling term in (3) and (5), a simple mixture model is used and the coupling drag is

$$\mathbf{D}_{ws} = C_D^* (v_s \rho_s + v_w \rho_w) v_s v_w |\mathbf{V}_w - \mathbf{V}_s| (\mathbf{V}_w - \mathbf{V}_s), \quad (6)$$

where C_D^* is a drag coefficient.

There exists no unique constitutive model for the rheology of submarine slides. Depending on the soil composition, different flow regimes govern the flow behavior, ranging from a more granular type in the case of low clay content to an increasingly visco-plastic behavior with increasing clay content. Norem et al. (1990) and Locat & Lee (2002) give an overview of various proposed models. For example, Gauer et al. (2005) used a

history-dependent Bingham fluid to model retrogressive sliding in the case of the Storegga Slide. For this study, we focus on the back-calculation of laboratory experiments with high clay content. In the tests, the material was stirred to achieve a homogeneous remolded mixture before release. For that reason, we disregard any strain-softening effects and use a simple Bingham fluid. For the purpose of modeling, the stress-strain relationship is written in the form of a generalized Newtonian fluid (Balmforth & Craster 2001):

$$\mathbf{T} = \mu_s(Y, \dot{\mathbf{D}}) \dot{\mathbf{D}}, \quad (7)$$

where \mathbf{T} is the deviatoric stress tensor, $\dot{\mathbf{D}}$ the rate of strain (deformation) tensor, and $\dot{\mathbf{D}} = -\frac{1}{2} \text{tr}(\dot{\mathbf{D}}^2)$ is its second invariant. In imitation of a Bingham fluid, the effective viscosity reads as

$$\mu_s = \frac{Y}{\dot{\gamma}} + K(Y), \quad (8)$$

where Y is the Yield strength, K the consistency, and $\dot{\gamma} (= 2\sqrt{-\dot{\mathbf{D}}})$ is the equivalent shear rate. In accordance with Locat and Demers (1988), the consistency is related to the yield strength by

$$K = \frac{Y}{1000} \text{ (Pa s)}. \quad (9)$$

Numerical simulation and comparison with laboratory experiments

The laboratory experiments were carried out at the St. Anthony Falls Laboratory, University of Minnesota. They are described in detail by Ilstad et al. (2004a, b, c). Figure 2 shows the principal setup of the experiments. Most experiments were performed

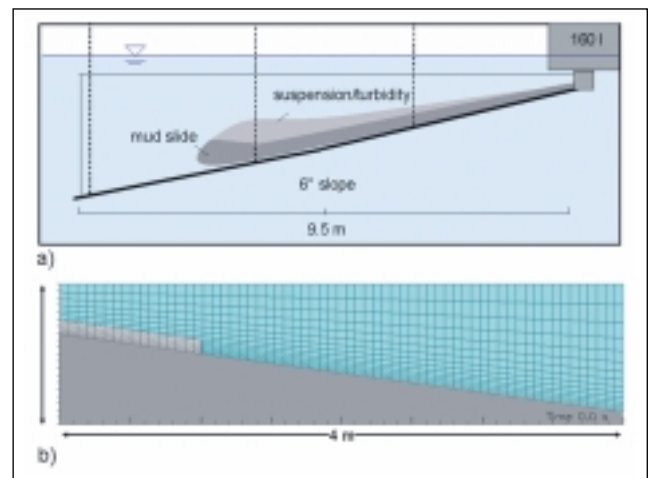


Fig 2: a) Schematic view of the experimental setup. b) Grid of the calculation domain and setting of the initial slab. The grid is thinned-out by a factor 5.

in a 0.2 m wide and 9.5 m long channel suspended in a larger glass-walled water tank. For the experiments back-calculated in this study, the slope of the sliding surface was kept to 6°. In all experiments, premixed and stirred slurry was released into a flume from a 160 l reservoir by rapidly opening an approximately 5.5 cm high gate. The setting for the numerical study differs slightly from the experimental setup. Here, we focused only on the development along the first 3 m of the channel. In addition, we simulate the slide release as a slab with an initial depth of 10 cm, in contrast to a flow from a reservoir. This should be kept in mind when directly comparing the results of the experiments with those of the numerical simulations. The experimental slide gains a considerable amount of potential energy from the raised reservoir, which is probably most important shortly after release. This fact might also partly explain why the yield strength used in the simulations needed to be lower than the one initially measured in the laboratory. However the derived yield strengths during the later stages of the flow (Ilstad 2004b) are similar to those used in the simulations. The initial setting of the numerical grid is also shown in Figure 2b. For a better illustration, the number of grid cells, which are shown in the figure, are reduced by a factor of 5 in comparison to the grid used in the simulation. The calculation domain was resolved by 320×75 volume cells; in this way, the horizontal resolution was approximately 1.25 cm and the vertical resolution close to the sliding surface was approximately 3 mm.

Figure 3 shows a time-lapsed sequence of video snapshots taken from a fixed position along the channel. The position was 7.6 m down from the inlet gate and the head structure was fully developed. Two things attract attention, i) the foremost part of the head is hydroplaning and ii) behind the head, water pockets get enclosed between the sliding surface and the sliding mass as the slide passes by. The first feature is described by Mohrig et al. (1998) and by Harbitz et al. (2003). The consequences of the latter feature are not fully understood. However, it is known that the shear strength strongly depends on the water content (Locat & Lee 2005; Cossout 1997). Hence, the enclosed water might contribute to a decrease of shear strength at the base of the sliding mass as it is molded by shearing. Elverhøi et al. (2005) coined the term shear-wetting for this process. The process of shear-wetting was not taken into account in the present numerical study.

Figure 4 depicts a sequence of time steps from a numerical simulation shortly after release. One can observe the development of hydroplaning at the head. De Blasio et al. (2004) did similar simulations; however they considered a rigid body of finite length in a laminar flow. Mohrig et al. (1998) proposed the following

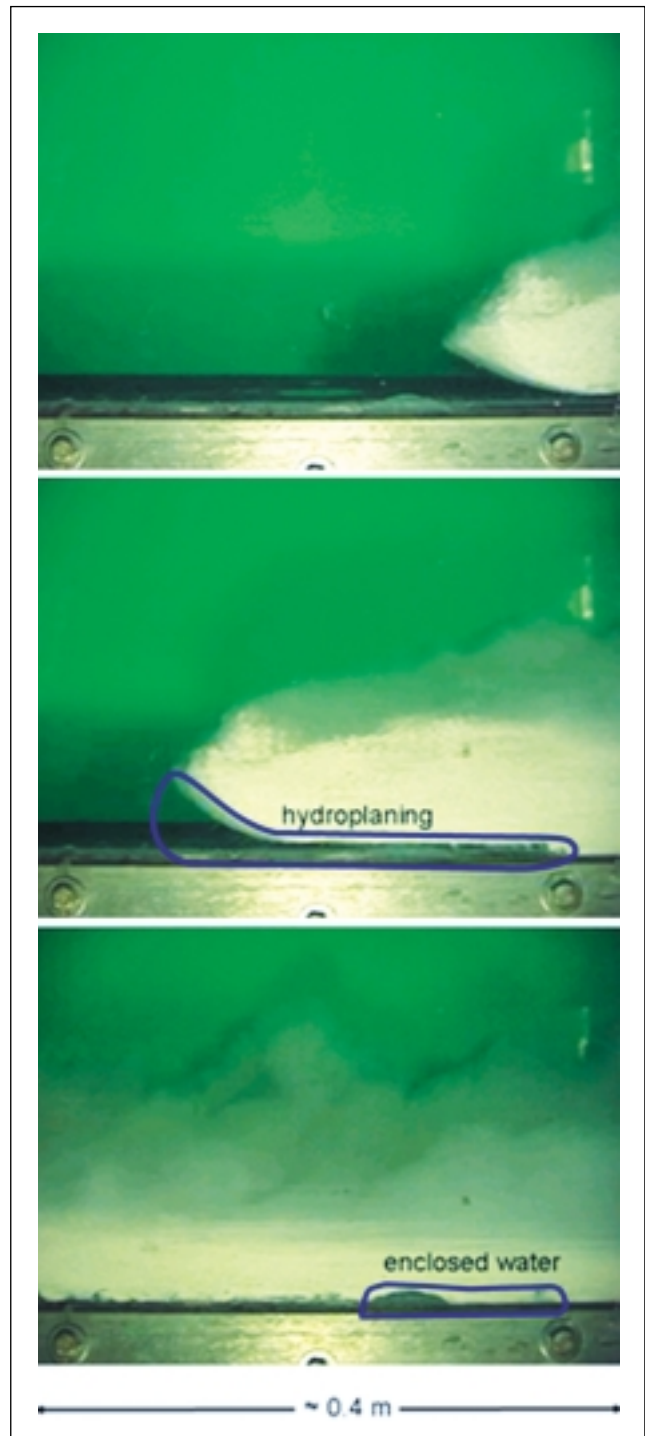


Fig 3: Snapshots of a video sequence taken at a fixed position about 7.6 m down the channel. The mixture was: water 35 %, sand 32.5 % and clay 32.5 % and density of 1690 kg m⁻³. The front velocity at this point is about 0.55 m s⁻¹.

relationship for the onset of hydroplaning:

$$U_c = \kappa \sqrt{2 \frac{(\rho_m - \rho_w)}{\rho_w} gh \cos \varphi} \quad (10)$$

where U_c is the critical velocity of the slide front at onset, h the thickness of the head, φ the slope angle,

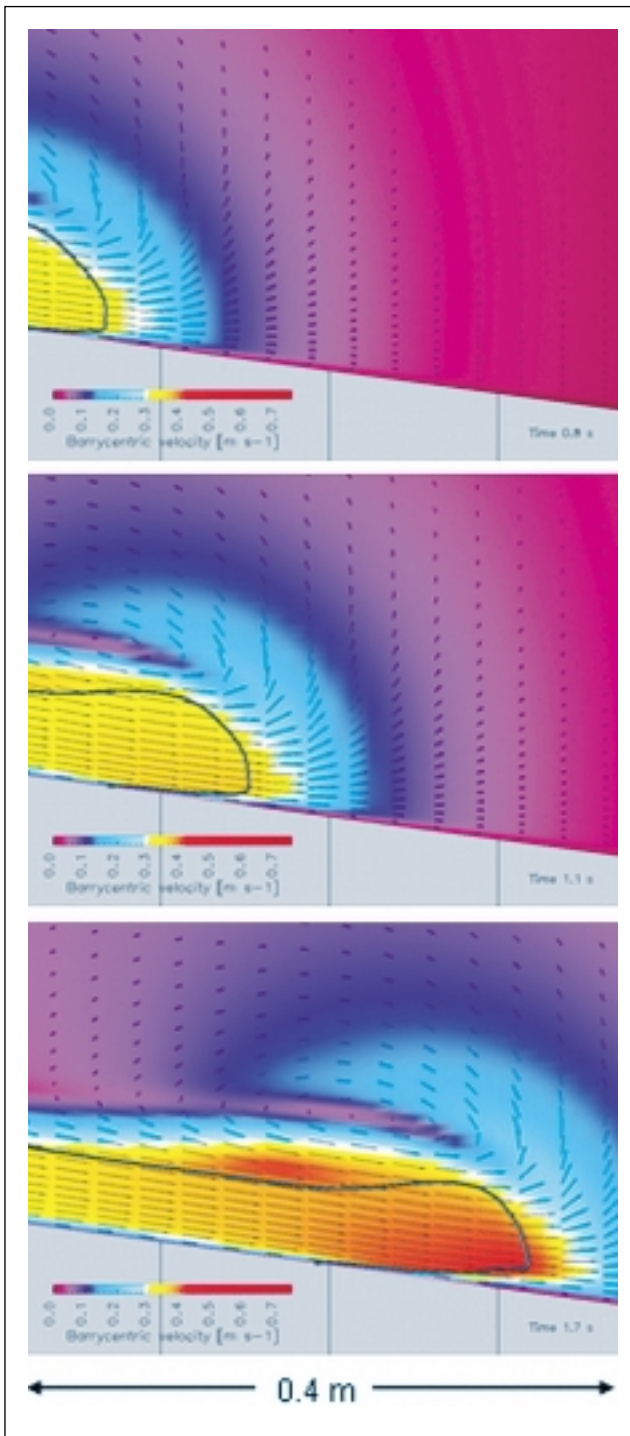


Fig 4: Back-calculation of laboratory experiments; three time steps shortly after release show the velocity field around the head. The bold line indicates the approximate surface of the slide marked by the 0.5 isosurface of the volume fraction. Vectors indicate the barycentric velocity field, and the speed is color coded. The yield strength, Y , in this simulation was 25 Pa.

and k is an empirical constant, which ranges between 0.3 and 0.4. The other symbols are defined above. Comparing this relationship with the simulation, we find a good agreement for the critical velocity. Figure 5 shows the development of a high-pressure wedge of ambient

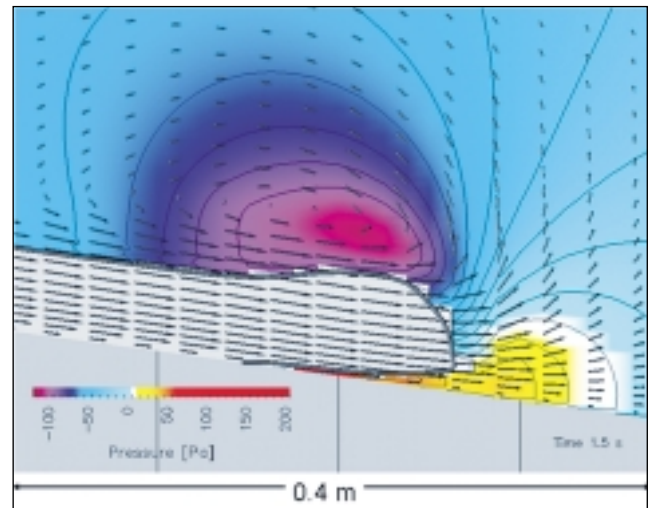


Fig 5: Back-calculation of laboratory experiments, snapshot at 1.5 s after release. Pressure field (color shaded), isobars black lines and velocity field (arrows) around the head of the slide. The bold line indicates the approximate surface of the slide marked by the 0.5 isosurface of the volume fraction.

water underneath the head of the slide and of under-pressure along its upper surface. The pressure difference constitutes a lift force, which is responsible for the onset of hydroplaning.

Further, in Figure 4, one can observe how the approaching slide displaces the ambient water in front of its head. The acceleration of the water causes a retarding force on the slide. In simple models like BING (Imran 2001), this effect has to be taken into account separately by a drag factor, as it is done in De Blasio et al. (2004). Otherwise, the slide velocity might be largely overestimated.

Another effect, which can be observed in the simulation, is stretching within the slide body. In Figure 4 one observes that beside the marked vertical velocity gradient, $\partial u_z / \partial z$, close to the sliding surface, there is also a noticeable horizontal gradient, $\partial u_x / \partial x$ (higher speeds at the front than in the following body). Usually this effect is disregarded in a one dimensional model. Hence, in those models using a Bingham rheology, the shear rate differs from that used in equation (8). In those cases, a simple plug is assumed that rides on top of a shear layer; this is an oversimplification. Figure 6 shows the equivalent shear rate (in a logarithmic scaling). First of all, one observes the high shear rate close to the sliding surface, as already mentioned above, with shear rates as high as 100 s^{-1} . However, instead of a "rigid" plug, plug-like zones are separated by zones in which stretching occurs. This stretching is especially pronounced between the hydroplaning head and the slide body. This zone might be prone to crack formation and even detachment. The high pressure below the hydroplaning head (especially at the transition to the non-hydropla-

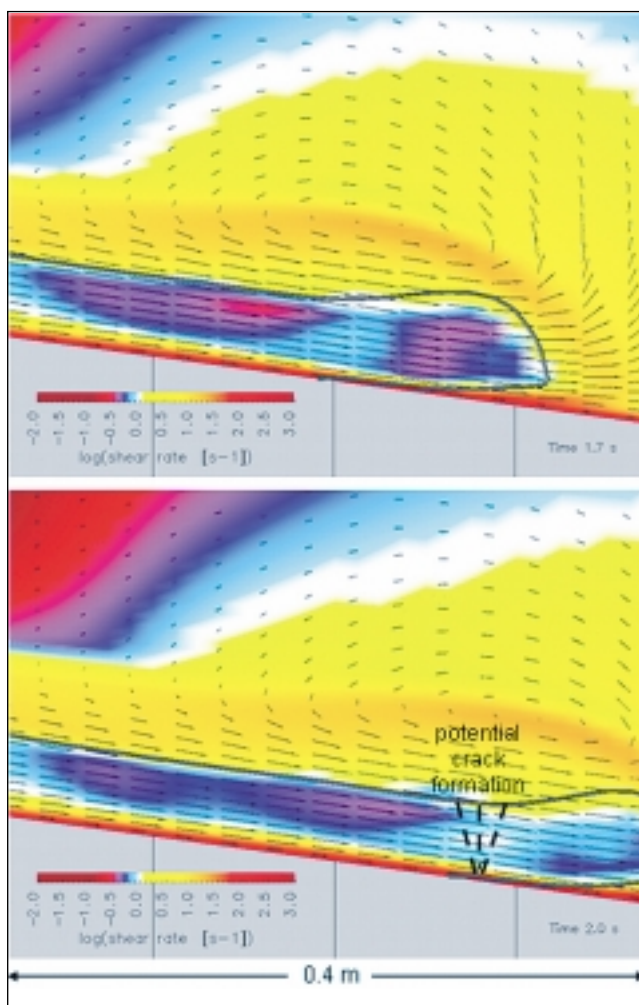


Fig 6: Equivalent shear rate, $\dot{\gamma} = \sqrt{2_{\dot{\epsilon}} - \dot{\epsilon}_D}$ (in a logarithmic scaling, color coded) for two time steps. Vectors indicate the corresponding velocity field.

ning body) might contribute to the crack formation. How this detachment occurs can be nicely seen in a photo sequence in (Ilstad 2004a, Fig. 5). The stretching itself causes remolding of the material that leads to a softening (if not already totally remolded), and so stretching may contribute to an increase of mobility. In addition, crack formation might lead to water intrusion, which enhances mobility by reducing the shear strength.

Concluding remarks

The numerical simulations resemble the laboratory experiments reasonably well. They also help to enlighten some of the basic concepts of slide movement—based on experimental and numerical studies—with a high clay content; a thin water layer might intrude underneath the front part forming a hydroplaning head. This thin water layer might also supply

water at the base of the remaining slide; in this case a shear-wetted basal layer develops with decreased yield strength enhancing the lubrication. This was not modeled in the presented study. In addition, stretching and thinning of material add to the softening of the material and, finally, may lead to progressive detachment of the head and development of out-runner blocks. However, not all of the effects are totally understood with all their consequences. One important question is to what extent does the intrusion of water underneath effectively enhance the runout? The introduction of a shear-wetting layer into numerical models constitutes a challenge, as this requires monitoring of the water content within the slide. A further challenge is the modeling of the detachment, which might require a different approach from that presented here. Furthermore, the laboratory experiments show that slides with lower clay content (less than 25%) behave quite differently from those modeled in this study. In cases with less than 25% clay, the sandy body seems to be partly fluidized by water infiltration. This fluidization, in contrast to the model used here, would be better described by a model that treats the slide material as a dispersed phase in the ambient water.

Acknowledgement: The International Centre for Geohazards (ICG) receives funding from The Research Council of Norway, which is gratefully acknowledged. This is paper number 99 of the ICG. We also acknowledge funding received from the Euromargin project (European Science Foundation 01-LEC-EMA14F). All numerical simulations were performed using ANSYS CFX4.4 flow solver. We also thank D. Moore and J. Marr for their thoughtful review.

References

- Bryn P, Berg, K., Forberg, C. F., Solheim, A. & Kvalstad, T. 2005: Explaining the Storegga Slide. *Marine and Petroleum Geology* 22, 11–19.
- Coussot, P. 1997. *Mudflow Rheology and Dynamics*. A. A. Balkema, Rotterdam, Netherlands.
- De Blasio F. V., Engvik, L., Harbitz, C. & Elverhøi, A. 2004: Hydroplaning and submarine debris flows. *Journal of Geophysical Research* 109, C01002, doi:10.1029/2002JC001714
- Elverhøi, A., Issler, D., De Blasio F.V., Ilstad T., C. B. Harbitz, C. B., & Gauer, P. 2005: Emerging insights on the dynamics of submarine debris flows. *Natural Hazards and Earth System Sciences* 5, 633–648.
- Ferziger, J. H. & Perić, M. 1999: *Computational methods for Fluid Dynamics*. 2nd rev. Edition. Heidelberg, Springer.
- Gauer, P., Kvalstad, T. J., Forsberg, C. F., Bryn, P. & Berg, K. 2005: The last phase of the Storegga Slide: simulation of retrogressive slide dynamics and comparison with slide-scar morphology. *Marine and Petroleum Geology* 22, 171–178.
- Harbitz, C. B., Parker, G., Elverhøi, A., Marr, J. G., Mohrig, D. & Harff, P. A. 2003: Hydroplaning of subaqueous debris flows and glide blocks: Analytical solutions and discussion. *Journal of Geophysical Research* 108, 2349–2366.
- Ilstad, T., De Blasio, F. V., Elverhøi, A., Harbitz, C. B., Engvik, L., Longva, O. & Marr, J. G. 2004a: On the frontal dynamics and morphology of submarine debris flows, *Marine Geology* 213, 481–497.
- Ilstad, T., Elverhøi, A., Issler, D. & Marr, J. G. 2004b: Subaqueous

- debris flow behavior and its dependence on the sand/clay ratio: a laboratory study using particle tracking, *Marine Geology* 213, 415–438.
- Ilstad, T., Marr, J. G., Elverhøi, A. & Harbitz, C. B. 2004c: Laboratory studies of subaqueous debris flows by measurements of pore-fluid pressure and total stress, *Marine Geology* 213, 403–414.
- Imran, J., Harff, P. & Parker, G. 2001: A numerical model of submarine debris flows with graphical user interface. *Computers Geoscience* 27, 717–729.
- Locat, J. & Lee, H. 2002: Submarine landslides: advances and challenges *Canadian Geotechnical Journal* 39, 193–212.
- Locat, J. & Lee, H. 2005: Subaqueous debris flows. In Jacob, M. & Hung, O. (Eds.), *Debris flow hazards and related phenomena*. Springer and Praxis, 203–245.
- Locat, J. & Demers, D. 1988. Viscosity, yield stress, remoulded strength, and liquidity index relationships for sensitive. *Canadian Geotechnical Journal* 25, 799–806.
- Mohrig, D., Whipple, K. X., Hondzo, M., Ellis, C. & Parker, G. 1998: Hydroplaning of subaqueous debris flows. *Geological Society of America Bulletin* 110, 387–394.